Hindawi
Advances in Civil Engineering
Volume 2021, Article ID 6954576, 16 pages
https://doi.org/10.1155/2021/6954576

Research Article

Static Topology Optimization and Dynamic Characteristics Analysis of 6000T Compression-Shear Test Machine Frame

Genshang Wu,[1] **Beibei Cui**,[2] **Yanmin Li**,[2] **Jinggan Shao**,[1] **Zhanshu He**,[2] **Shusen Zhao**,[2] **Chao Li**,[2] **and Jinlong Yu**[2]

[1]*Highway Institute, Henan College of Transportation, Zhengzhou 450005, China*
[2]*School of Mechanical and Power Engineering, Zhengzhou University, Zhengzhou 450001, China*

Correspondence should be addressed to Yanmin Li; ymli64@zzu.edu.cn and Zhanshu He; hezhanshu@zzu.edu.cn

Received 2 August 2021; Revised 27 September 2021; Accepted 12 October 2021; Published 29 October 2021

Academic Editor: Fabio Di Trapani

This work aims to achieve the 6000t compression-shear test machine frame design with the lightweight. The force condition of the compression-shear test machine frame under limited working conditions is first analyzed, and the static analysis of the compression-shear test machine frame is performed using ABAQUS. Then, taking the volume of the frame of the compression-shear testing machine as the constraint condition, the topology optimization of the compression-shear testing machine frame is performed using the variable density method of topology optimization, and the model is reconstructed accordingly. Finally, not only the static characteristics of the frame before and after optimization but also the modal characteristics of the frame before and after optimization and the dynamic characteristics after sudden unloading are compared and analyzed. The results show that the weight of the frame decreases by 14.5% after optimization, and the maximum static stress of the frame is still less than the yield strength of the material; the maximum displacement is still less than the allowable maximum displacement, which meets the requirements of static strength and stiffness. The natural frequency of each mode is much greater than the working frequency, which meets the requirements of dynamic stiffness. After sudden unloading, the maximum dynamic stress of beams, columns, and base of the frame are less than the yield strength of materials, which meets the requirements of dynamic strength.

1. Introduction

The mechanical properties of bridge rubber bearings have a great influence on the life and safety of bridges, highways, and other engineering facilities [1, 2], so compression-shear test machines are usually used to test their mechanical properties before engineering application. In recent years, the load on bridge bearings is gradually increasing, so the tonnage of compression-shear test machine is also increasing, and its frame weight is also greatly increasing. The conservative design of the compression-shear test machine frame based on experience may result in a great waste of materials. Thus, it is necessary to perform the topology optimization of the compression-shear test machine frame using finite element software, so as to reduce the weight as much as possible on the premise of ensuring the mechanical properties [3–5].

Domestic and foreign scholars performed topology optimization and mechanical analysis on different types of test machines using finite element software, so as to achieve the test machines with the lightweight. Wang et al. [6] performed static and modal analysis of the electrohydraulic servo test machine column using Hyper Mesh software and performed the topology optimization based on the analysis results. The results showed that the optimized column still met the requirements of static strength and dynamic stiffness, and the weight reduced by 6.58%. Xue et al. [7] performed the static analysis on the connecting rod of hydraulic fatigue test machine under two ultimate forces of tension and compression using ANSYS, and they performed the topology optimization of the connecting rod accordingly. The results showed that the optimized connecting rod weight reduced by 8.2% and still met the requirements of static strength. Feng and Luo [8] performed the static and

modal analysis on the movable end fixture and transmission spindle of concrete temperature-stress test machine using ANSYS and performed the topology optimization of the two parts. The results showed that the weight of the optimized movable end fixture and transmission spindle reduced by 14.8% and 21.6%, respectively. Du and Olhoff [9] performed the problems of topology optimization with respect to eigenfrequencies of free vibrations of structures. The results showed that the method developed enabled us, in a cost-efficient manner, to move structural resonance frequencies far away from external excitation frequencies and thereby avoid high vibration and noise levels. Kazakis et al. [10] performed a novel topology optimization-aided structural design methodology where topology optimization is integrated with an interpretation step. The proposed methodology was based on a fully automated design procedure. Di Trapani et al. [11] proposed an optimization framework aimed at the minimization of seismic retrofitting-related costs by an optimal placement (topological optimization) and amount of steel-jacketing reinforcement. The results showed that the approach tested on simple frame structure was valid, which can effectively reduce reinforced concrete building retrofitting and downtime costs controlling safety levels above a specified value. Sotiropoulos et al. [12] proposed a general method for addressing the topic of conceptual design by means of topology optimization and provided the capability to design structural systems that cannot be obtained through ordinary approaches. The proposed method was successfully applied to 2D and 3D problems. Di Trapani et al. [13] proposed that a new specific optimization framework addressing the minimization of seismic retrofitting-related costs to be developed and presented. A new genetic algorithm routine is defined by developing modified genetic operators capable of addressing retrofitting optimization both for reinforced concrete structures with ductility-critical and shear-critical reinforced concrete columns, including additional shear demand due to infill-frame interaction. The results showed that the proposed approach was sufficiently general and robust to handle structural configuration having significantly different structural deficiencies. Rosso et al. [14] proposed a new nonpenalty-based constraint handling approach for particle swarm optimization, adopting a supervised classification machine learning method, the support vector machine. The results showed that the new approach represented a valid alternative to solve constrained optimization problems even in structural optimization field. Cucuzza et al. [15] discussed about optimal shape solution for a non-prismatic planar beam. The proposed model was based on the standard Timoshenko kinematics hypothesis (i.e., planar cross section remains planar in consequence of a deformation, but it was able to rotate with respect to the beam center line). The results showed that the study found a critical threshold in terms of emptying function, beyond which, it is not possible to neglect the arch effect and the curvature of the actual axis for every different case study described in this work.

Besides the test machine, domestic and foreign scholars had performed topology optimization and mechanical analysis on other large machines, and a lightweight is realized. Wang et al. [16] proposed a new topography optimization method called "windowed progressive structure optimization algorithm" and established the tie rod-compression rod model reflecting the working mechanism of the structure. The results showed that the topological optimal solution obtained by the windowed progressive structure optimization algorithm can better represent the internal stress state of the structure; by the optimization method, the opening ratio of I-beam structure is increased by 5.5 times compared with the experimental design, the ultimate load is increased by 1.2 times, but the amount of steel reduced by 30%. Kong et al. [17] proposed the combination of topology and topography methods to simulate weight optimization of coil spring lower seat design. The results showed that the induction of topographical beads on the component had resulted in the strengthening of the lower seat design with minimum acquired material while reducing the mass by 36.5%. Li et al. [18] proposed the mathematical model of the lightweight optimization design and established the geometric model of the initial design of the front upright. The results showed that the structural optimization of a front upright resulted in the weight reduction of the upright by 60.4%. Deng and Sun [19] proposed the topology optimization based on gradient threshold, the design variables were considered to be sizing, which were plate's thickness and rib's section area, and the fully stressed design (FSD) criterion were adopted as optimization strategy to obtain the optimal solution. Numerical results of several examples expressed that on the condition of the equal structural stiffness, the proposed method could reduce the structural weight from 5% to 20% compared with the traditional approach based on engineering experience. Zhang et al. [20] performed the variable density topology optimization method to calculate the stress distribution of the trimaran bulkhead structure under different working conditions. The results showed that the optimization could reduce 50% of the structure weight in the optimization area of the bulkhead and realize the lightweight design of the non-watertight bulkhead structure, under the premise of ensuring safety of the structure. Resmy and Rajasekaran [21] proposed the topology optimization of 3D concrete dapped beams using a bidirectional evolutionary structural optimization method within the environment of ABAQUS finite element software. The results showed that objective history was different for all the load cases, although lateral load case took more iteration steps to converge. Final topology like truss pattern had arrived after a reasonable number of iteration, which could be utilized for the appropriate generation of the strut and tie modeling. Wang et al. [22] performed the topology optimization to the civil aircraft structure, so as to reduce the weight. The results showed that the topology optimization structure achieved a weight reduction of 25% and a structural stiffness increasing of 75.7% compared with the traditional structure. Xie et al. [23] performed the lightweight design to the hydraulic valve block based on the multiobjective topology optimization method. The results showed that when compared with the original model, after optimization the maximum stress of the final design corresponds to 542.9 MPa, which satisfied the material strength requirement, and the weight decreased by 68.9%.

However, most of the topology optimization machines in the above literatures are small in tonnage, and do not reach the kiloton level. The compression-shear test machine studied in this article reaches 6000t, which sustains great stress. The frame weight is also very large, so it is necessary to perform the topology optimization to achieve lightweight. In addition, most of the above literatures only perform the static and modal analysis to verify whether the static strength, static stiffness, and dynamic stiffness meet the requirements, but those are not enough for the test machine. The sudden fracture of the specimen (i.e., the test machine after sudden unloading) will have a great impact on the frame, and the dynamic stress at a certain time may be greater than the static stress under static loading. Moreover, the compression-shear test machine studied in this article sustains both horizontal and vertical loads, and the dynamic stress after sudden unloading is more complex, so it is very necessary to analyze the dynamic characteristics after sudden unloading and verify that whether the dynamic strength meets the requirements. However, there are few literatures related studies, only Chu et al. [24] analyzed the dynamic characteristics of small tonnage tension-compression test machines after sudden unloading only in the tensile working condition (only sustaining vertical load). It has not been found that the dynamic characteristics of the testing machine with large tonnage and simultaneous loading in multiple directions have not been analyzed after sudden unloading. This study aimed to achieve the 6000t compression-shear test machine frame design with lightweight. The force condition of the compression-shear test machine frame under limited working condition is analyzed, and the static analysis of the compression-shear test machine frame is performed using ABAQUS. Then, taking the volume of the frame of the compression-shear testing machine as the constraint condition, the topology optimization of the compression-shear testing machine frame is performed using the variable density method of topology optimization, and the model is reconstructed accordingly. Finally, not only the static characteristics of the frame before and after optimization but also the modal characteristics of the frame before and after optimization and the dynamic characteristics after sudden unloading are compared and analyzed.

2. Topology Optimization of Variable Density Method (Solid Isotropic Microstructures with Penalization, SIMP)

2.1. Establishing an Optimization Model. Topological optimization aims to achieve the optimal material distribution of the structure by iterative calculation in a given optimization region, combined with boundary conditions. In the process of topology optimization, element density is usually selected as the design variable, and its mathematical model is expressed as follows:

$$\begin{aligned} X &= [x_1, x_2, x_3, \ldots, x_n]^T, \\ F(X) &\longrightarrow \min(\text{or}\max), \\ h_j(x) &= 0, \quad j = 1, 2, 3, \ldots, k, \\ G_1(x) &\leq 0, \quad i = 1, 2, 3, \ldots, m, \\ X &\geq 0, \end{aligned} \tag{1}$$

where, X is the design variable, $F(X)$ is the objective function, $h_j(x)$, and $G_I(x)$ should meet the constraints in the process of topology optimization (i.e., h_j and G_i are the response constraints, such as stress level and displacement).

In this article, the variable density topology optimization method is used to optimize the frame of the compression-shear test machine. The cell density of each cell in the optimization model is taken as a design variable, and the value is continuously between 0 and 1. In the optimization process, the area where the unit density is close to 1 is reserved, and the area where the unit density is close to 0 is deleted, so as to achieve the optimal material distribution of the compression-shear test machine frame [25].

2.2. Design Sensitivity. Before quantitative design decisions can be made, there must be a design sensitivity analysis. Sensitivity derivative information is a kind of evaluation of structural response due to a design variable or parameter changes of the rate of change. Structure sensitivity study is the current structural mechanics and one of the main research directions in the field of structural engineering. Sensitivity analysis can obtain the variation relationship between the structural response and design variables of the compression-shear testing machine frame, which can significantly improve the optimization efficiency. The direct method adopted in this article is suitable for optimization problems with many constraints and few design variables [26].

The approximate display model is established by solving the sensitivity, and the small step is used for iterative solution. This iteration is completed when the error of the target value of two consecutive iterations is less than the given convergence tolerance (the default value is 0.005).

The design sensitivity is the partial derivative of the response optimization variable (X is the design variables, such as cell density):

$$KU = P, \tag{2}$$

where K is the stiffness matrix, U is the element displacement vector, and P is the element load vector.

Partial derivatives of the design variable X on both sides of the equation can be obtained as follows:

$$\frac{\partial K}{\partial X}U + K\frac{\partial U}{\partial X} = \frac{\partial P}{\partial X}. \tag{3}$$

Then, partial derivative of the displacement vector U can be obtained as follows:

$$\frac{\partial U}{\partial X} = K^{-1}\left(\frac{\partial P}{\partial X} - \frac{\partial K}{\partial X}U\right). \tag{4}$$

The design response is generally a displacement (i.e., U) function:

$$g = Q^T U, \tag{5}$$

where g is the constraint function and Q is the adjoint load vector.

Partial derivatives of the design variable X on both sides of the equation can be obtained as follows:

$$\frac{\partial g}{\partial X} = \frac{\partial Q^T}{\partial X}U + Q^T\frac{\partial U}{\partial X}. \tag{6}$$

For topology optimization, the adjoint variable method is usually used to calculate sensitivity. The adjoint variable E is introduced to satisfy the following equations:

$$\begin{aligned} KE &= Q, \\ \frac{\partial g}{\partial X} &= \frac{\partial Q^T}{\partial X}U + E^T\left(\frac{\partial P}{\partial X} - \frac{\partial X}{\partial X}U\right). \end{aligned} \tag{7}$$

2.3. Optimization Criterion. In the optimization process, in order to make the stress distribution of the structure more uniform, the maximum stress is within the specified stress limit, and the material weight or volume is the smallest; a topological optimization method considering stress and stress sensitivity distribution information is established by fitting the criteria of gradient descent method and traditional progressive structural optimization method. Generally, stress uniformity is maintained by deleting small stress elements and adding high stress artificial material elements. Secondly, when adding or deleting elements, in order to make the stress variation of other elements caused by the addition or deletion of this element as small as possible, the element with small absolute value of stress sensitivity should be selected for addition or deletion [27].

Therefore, the optimization method criterion can be described as follows: select the element of n_d with the smallest absolute value of the stress sensitivity number to delete the region of the small stress (the number of elements (i.e., n_r) in this region); select a certain number of n_a elements with the smallest absolute value of stress sensitivity number to increase the region of the higher stress (the number of elements (i.e., n_s) in this region) until the stress limit is reached. Where, $n_d = \min(RS_d, N_v, n_r)$, $n_a = \min(RS_a, N_v, n_s)$, structure retained material unit number is N_v, v is the optimization iterations, RS_d is the unit removed rate based on the stress sensitivity (that is, the current number of structural units multiplied by the unit deletion rate is the number of deleted units, which is generally set to 0.01), and RS_a is the element addition rate based on the stress sensitivity (that is, the current number of structural units multiplied by the addition rate is the number of added units, which is generally set to 0.01).

3. Static Topology Optimization of 6000t Compression-Shear Test Machine Frame

3.1. Force Analysis of 6000t Compression-Shear Test Machine Frame. Figure 1 shows the structure drawing and technical drawing of 6000t compression-shear test machine, which mainly includes the upper beam, column, base, workbench, vertical loading system, and horizontal loading system. The upper beam, column, and base are installed together to form the compression-shear test machine frame, the workbench is placed on the base, the vertical loading system is installed on the upper beam, and the horizontal loading system is installed on the oil cylinder seat of the base. In the test, if the specimen is firstly placed on the workbench, then the vertical cylinder in the vertical loading system moves up and down, and the vertical load is applied to compress the specimen, then the transverse cylinder in the transverse loading system moves left and right, and the transverse loading system is applied to the specimen for shearing. The maximum vertical load, the maximum lateral load, and the maximum horizontal displacement of the 6000t compression-shear test machine are 60 MN, 9 MN, and 800 mm, respectively.

Next, the force output from the vertical cylinder and the transverse cylinder are loaded to the corresponding position, and the stress of the specimen in the compression-shear process is analyzed, as shown in Figure 2. Because the friction between the bottom and the base of the workbench is small, it is ignored. According to the principle of static balance, the structure is subjected to two pairs of loads (i.e. the transverse load and the vertical load).

(1) The vertical load satisfies the following equation:

$$P = N_1 + N_2, \tag{8}$$

where P is the force exerted by the vertical cylinder on the specimen and N_1 and N_2 are the forces exerted by the base on the specimen. P, N_1, and N_2 reach static equilibrium to compress the specimen. For the frame, P will also produce reaction force on the upper beam of the frame, and N_1 and N_2 will also produce reaction force on the base of the frame. P, N_1, and N_2 will also achieve static balance in the vertical direction of the frame.

(2) The transverse load satisfies the following equation:

$$F_1 = F_2, \tag{9}$$

where F_1 is the force exerted by the transverse cylinder on the specimen, and F_2 is the force exerted by the column on the specimen. F_1 and F_2 reach static balance to shear the specimen. For the frame, F_1 will also produce a reaction force on the oil cylinder seat on the frame base, and F_2 will also produce a reaction force on the column. F_1 and F_2 will also achieve static balance in the horizontal direction of the frame.

We assume that the movement distance of the workbench is x, and the distance between the center line of the pressure action of the horizontal cylinder and the reaction

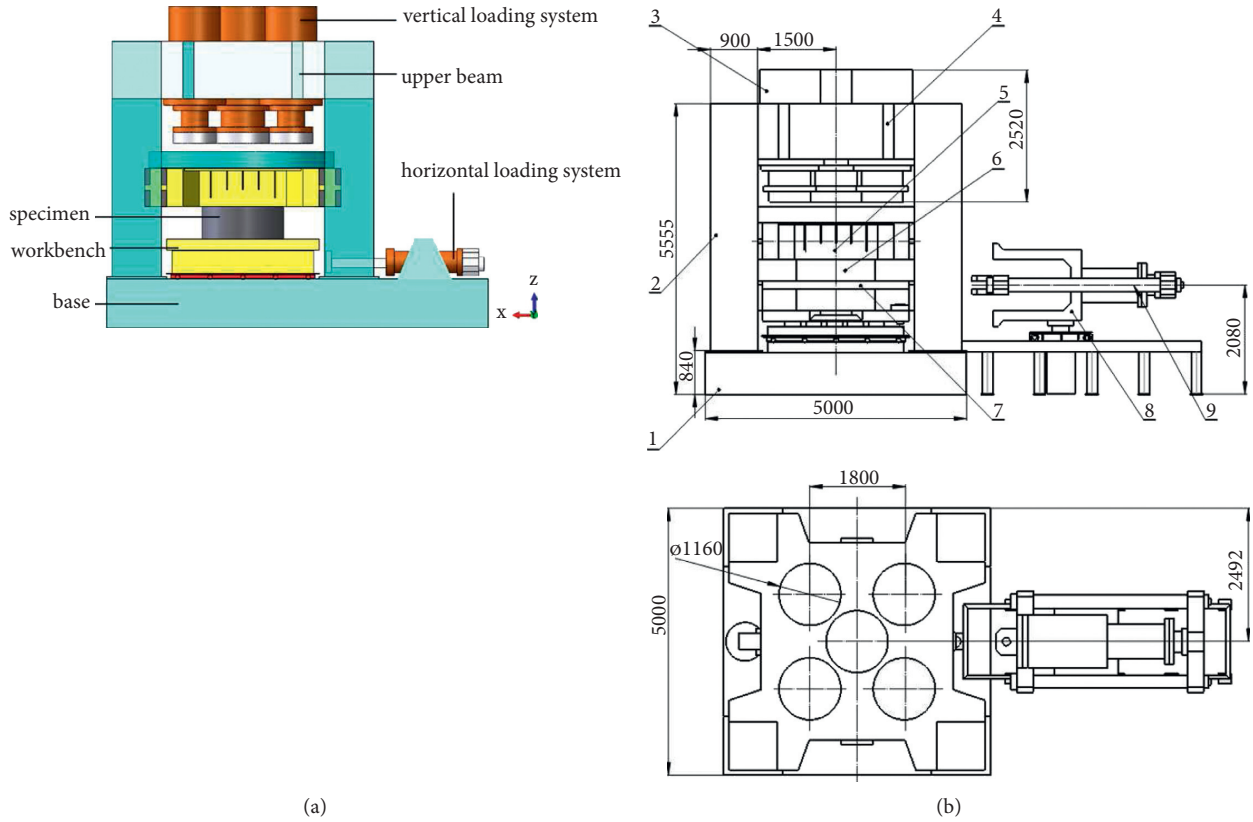

(a) (b)

FIGURE 1: Structure drawing and technical drawing of 6000t compression-shear test machine. (a) Overall layout of 6000t compression-shear test machine. (b) Technical drawing of 6000t compression-shear test machine. (1) Base; (2) column; (3) hydraulic cylinder; (4) upper beam; (5) upper platen; (6) specimen; (7) cylinder; (8) double shear plates.

force of the moving crossbeam is H. Half of the distance of the rolling slider under the workbench is L. Then, the equation can be obtained from the moment balance:

$$N_2(L-x) = N_1(L+x) + F_2H. \tag{10}$$

N_1 and N_2 can be solved by combining the above equations:

$$N_1 = \frac{[P(L-x) - F_2H]}{2L}, \tag{11}$$

$$N_2 = \frac{[P(L+x) + F_2H]}{2L}. \tag{12}$$

When P reaches the maximum vertical load of 60 MN, F_1 reaches the maximum lateral load of 9 MN, and x reaches the maximum horizontal displacement 800 mm of the workbench. At this moment, the compression-shear test machine frame is under the ultimate working condition. These parameters can be substituted in equations (11) and (12); it can be obtained that $N_1 = 7.24$ MN, $N_2 = 52.76$ MN.

3.2. Topology Optimization of 6000t Compression-Shear Test Machine Frame. Based on the force analysis under the above ultimate working conditions, the static analysis of the compression-shear test machine frame is performed using ABAQUS. Before the analysis, it is necessary to simplify the 3D model of the frame properly. Firstly, the cylinder in the system is simplified, and the force output from the cylinder is loaded to the corresponding position; then, the bolted connection between the two parts is deleted, and the node coupling method is used to calculated. Then, the hole features such as technological hole, locating hole, threaded hole, and tiny chamfer and fillet are deleted. Finally, the simplified 3D model of compression-shear test machine frame is obtained, and then, the simplified 3D model is imported into the ABAQUS. The frame material is Q345, its density is 7850 kg/m^3, young's modulus is 206 GPa, Poisson's ratio is 0.3, and yield strength is 345 MPa. As shown in Figure 3, the load is applied, and boundary constraints are set. The longitudinal force is applied to the bottom surface of the upper beam, with the magnitude of 60 MN and the direction along the z-axis. The reaction force is applied to the base with the magnitude of 60 MN, and the direction is negative along the z axis. Because the base is fixed on the ground, the base boundary is set to be completely fixed. Finally, the hexahedral element is used to mesh the model, and the static analysis begins.

Figure 4 shows the stress and displacement cloud diagram of the optimized front compression-shear test frame under ultimate working conditions. The maximum static stress of the compression-shear test machine frame before optimization is 204 MPa, which is at the contact position between the upper beam and the column, and the stress is less than the material

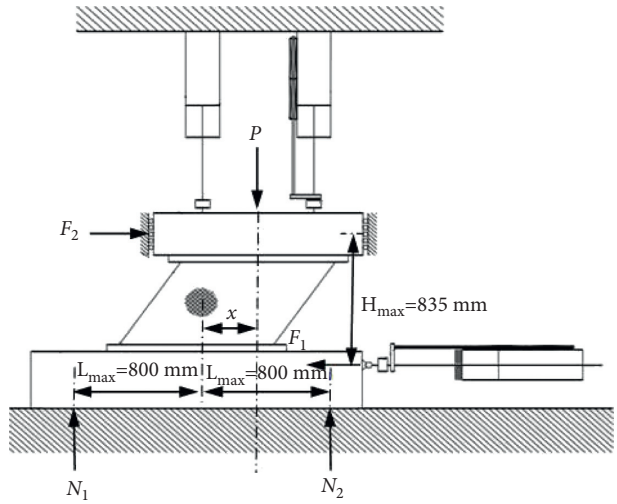

Figure 2: Force of the specimen in the process of compression and shear.

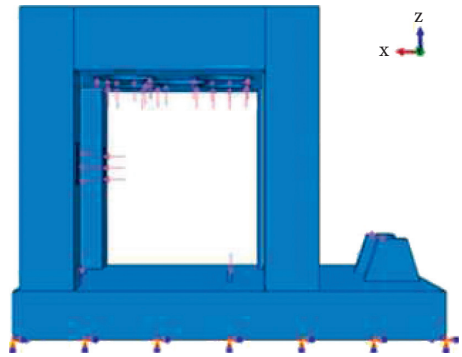

Figure 3: Simplified load and boundary constraints of the compression-shear test machine frame.

yield strength. The maximum displacement is 2.437 mm, which is at the upper edge of the upper beam where the upper beam is at the contact with the hydraulic cylinder, and the overall displacement is small. Although the compression-shear test machine frame meets the requirements of static strength and stiffness, there are a lot of low-force or zero-force elements on the vertical column and upper beam; there is still a large space for topological optimization.

Therefore, the 3D model of the compression-shear test machine frame is imported into the ABAQUS again, and the tetrahedral element grid is used to mesh the model. Then, the topology optimization is performed based on the static analysis results, as shown in Figure 4. The topology task is established in the optimization module, and the base of the compression-shear test machine frame is selected as the frozen area (i.e., the base is not optimized); the strain energy and volume design response are created, the objective function is strain energy, and then, the volume constraint was created to remove 30% of the material for calculation. The final result of topology optimization is shown in Figure 5.

According to the results of topology optimization, more materials are removed from the outer side of the column and the four corners of the upper beam, and most of them are irregular shapes. Considering the processing feasibility and assembly difficulty, the size and shape of the compression-shear test machine frame after topology optimization are slightly adjusted using SolidWorks, and then, the model is reconstructed. As shown in Figure 6, the weight of the compression-shear test machine frame reduces by 72239.1 kg after optimization and reconstructed.

Static analysis is performed on the optimized and reconstructed frame of the compression-shear test machine, as shown in Figure 7. The maximum static stress of the frame is 235 MPa at the contact position between the upper beam and the column, and the stress is still less than the yield strength of the material. The maximum displacement of the frame is 3.089 mm, which also is at the upper edge where the upper beam is in contact with the hydraulic cylinder, and the overall displacement is still small.

By comparison, the maximum static stress and maximum displacement of the optimized compression-shear test machine frame are slightly larger than those before optimization (Table 1); they are still less than the yield strength and the maximum allowable displacement of the material, respectively, and the weight reduced by 14.5%. Therefore, the topology optimization scheme achieves the lightweight of the compression-shear test machine frame on the premise of satisfying the static strength and stiffness.

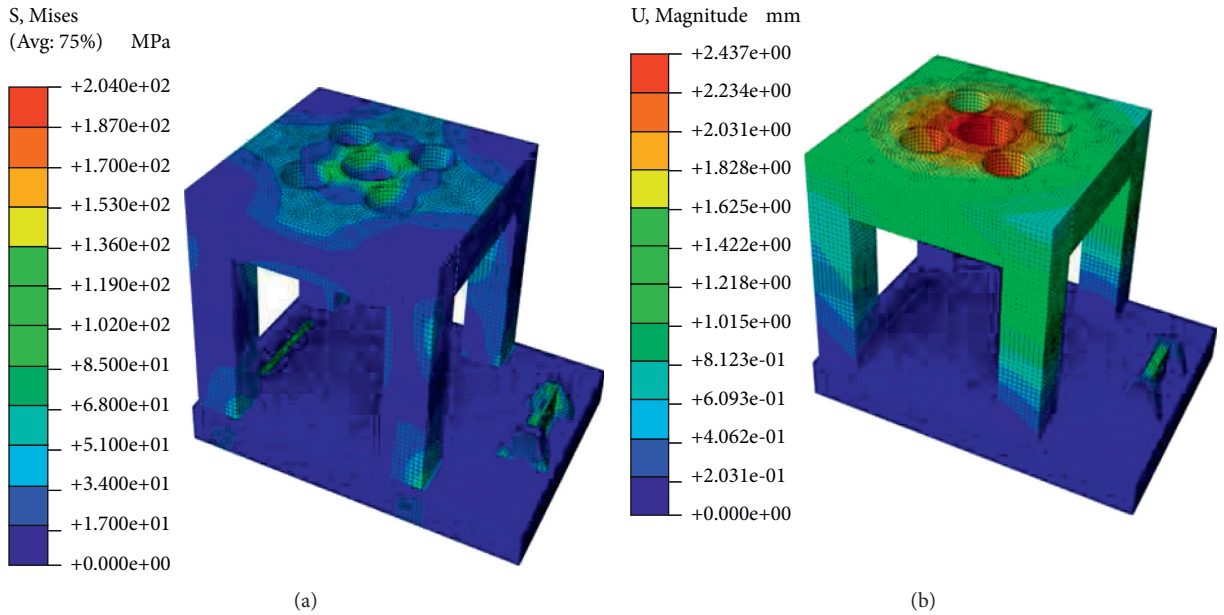

Figure 4: Stress and displacement cloud diagram of the compression-shear test machine frame under the ultimate working condition before optimization. (a) Stress cloud diagram. (b) Displacement cloud diagram.

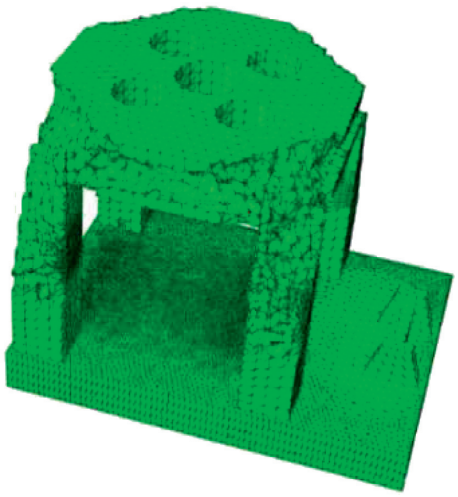

Figure 5: Final result of topology optimization.

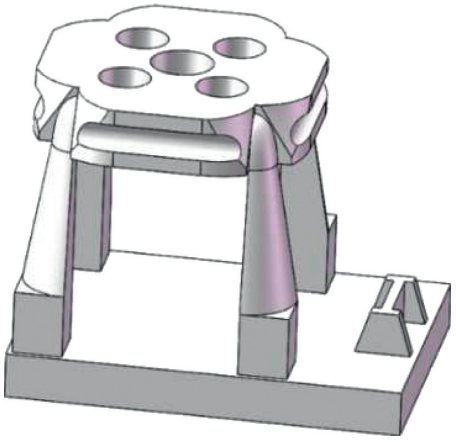

Figure 6: Optimized and reconstructed of compression-shear test machine frame.

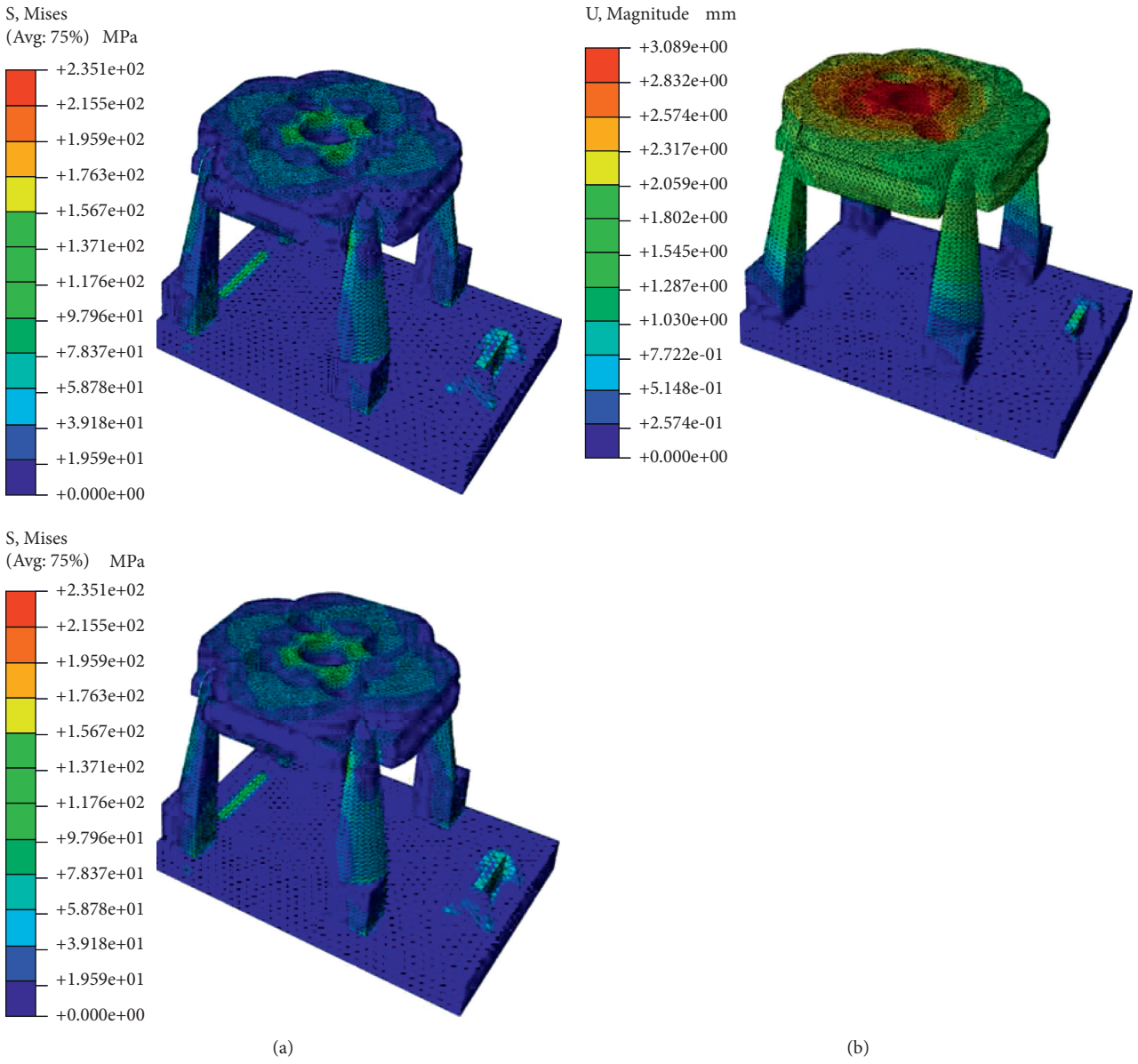

Figure 7: Stress and displacement cloud diagram of the optimized compression-shear test machine frame under the ultimate working conditions. (a) Stress cloud diagram. (b) Displacement cloud diagram.

4. Dynamic Characteristics of 6000t Compression-Shear Test Machine Frame

The following is the analysis and comparison of the modal characteristics of the compression-shear test machine frame and the dynamic characteristics after sudden unloading before and after topology optimization.

4.1. Modal Characteristics of the Frame. The 3D model of the original and optimized compression-shear test machine frame is imported into the ABAQUS, the analysis step type is selected as the frequency analysis step in linear perturbation, and the second-order tetrahedral element (C3D10) type is used for meshing, and then, modal analysis begins. Because the influence of low-order vibration mode on the structure is greater than that of higher-order vibration mode, this study only obtains the first four natural frequencies and vibration modes of the compression-shear test machine frame.

Figure 8 shows the modal analysis results of the compression-shear test machine frame before optimization; the first-order modal natural frequency is 24.384 Hz, which is mainly represented by the swing of the upper crossbeam in the *X*-*Y* plane. The second-order modal natural frequency is 24.626 Hz, which is mainly represented by the torsion of the upper beam and column in the *X*-*Y* plane. The third-order mode natural frequency is 34.189 Hz, which is mainly represented by the torsion of the upper beam and column in the *X*-*Y* plane. The fourth-order mode natural frequency is 90.815 Hz, which is mainly represented by the vibration of the upper beamalong the *Z* axis and the torsion of the column in the *X*-*Y* plane.

Table 1: Comparison before and after optimization-shear test machine frame.

	Maximum static stress (MPa)	Maximum displacement (mm)	Weight (kg)	Proportion of weight reduction after optimization (%)
Before optimization	204	2.437	497228.55	14.5
After optimization	235	3.089	424989.45	

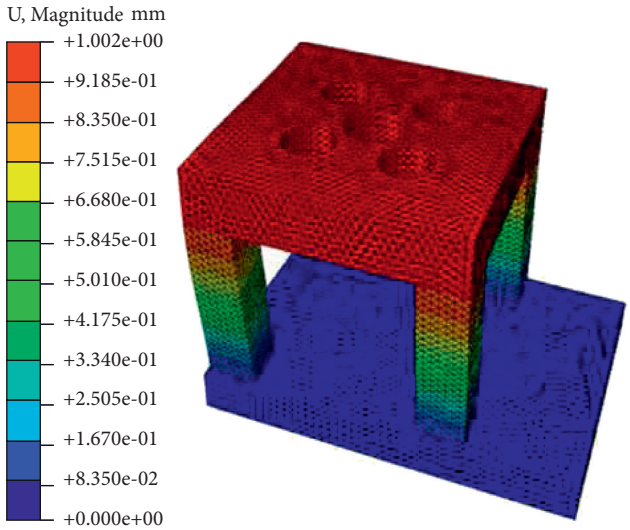

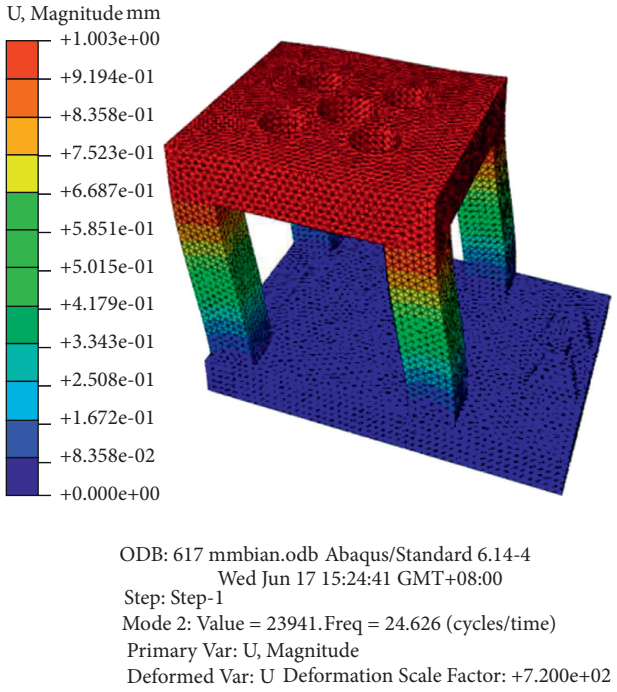

(a)

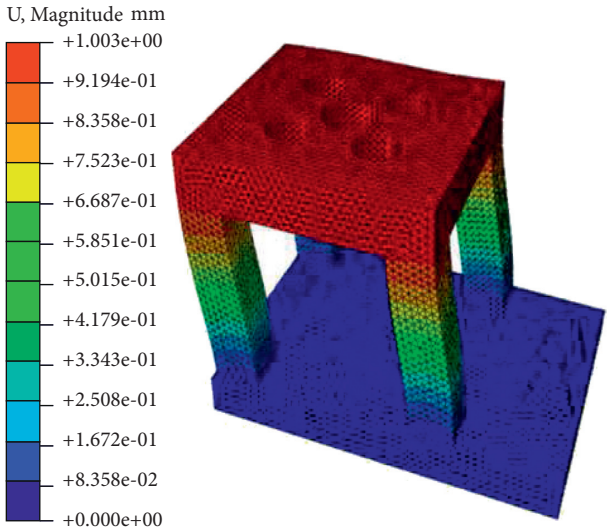

(b)

Figure 8: Continued.

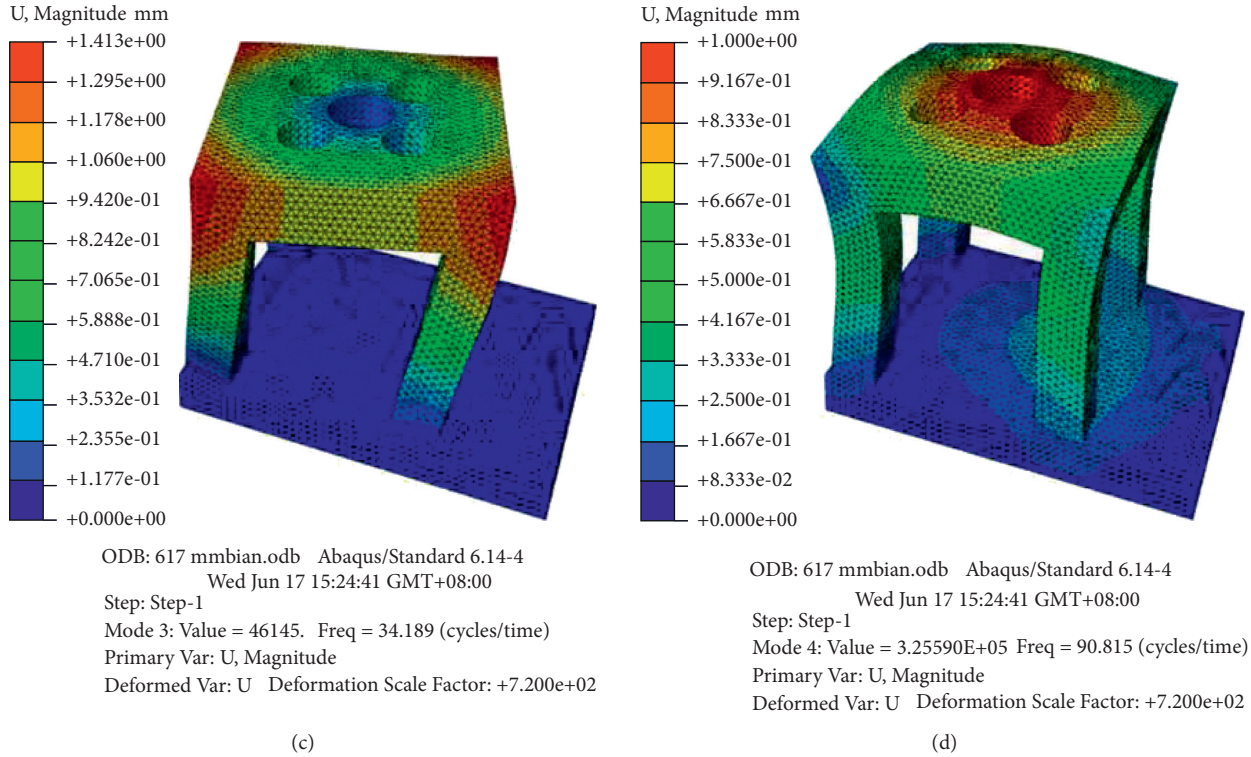

Figure 8: Modal analysis results of compression-shear test machine frame before optimization. (a) First-order mode. (b) Second-order mode. (c) Third-order mode. (d) Fourth-order mode.

Figure 9 shows the modal analysis results of the compression-shear test machine frame after optimization. The first-order mode natural frequency is 19.486 Hz, which is mainly represented by the swing of the upper beam in the X-Y plane. The natural frequency of the second mode is 19.631 Hz, which is mainly represented by the torsion of the upper beam and column along the Z axis. The third-order mode natural frequency is 27.942 Hz, which is mainly represented by the torsion of the upper beam and column in the X-Y plane. The natural frequency of the fourth-order mode is 88.313 Hz, which is mainly represented by the vibration of the upper beam along the Z axis and the torsion of the column in the X-Y plane.

By comparison, the instability modes of each mode of the original and optimized compression-shear test machine frame are basically unchanged. The natural frequencies of each mode after optimization are slightly smaller than those before optimization (Table 2), the values are still relatively large and much greater than the maximum working frequency 0.05 Hz, so no resonance will occur, and the frame also has relatively large dynamic stiffness. Therefore, the topology optimization scheme can reduce the weight of the compression-shear test machine frame on the premise of satisfying the dynamic stiffness.

4.2. Dynamic Characteristics after Sudden Unloading. The dynamic characteristics of the compression-shear test machine frame after sudden unloading are analyzed using ABAQUS with explicit dynamic analysis method, and the loading process is shown in Figure 10. During 0~0.01 s, the lateral force on the side of the column increases from 0 to 9 MN, and the lateral reaction force on the cylinder seat also increases from 0 to 9 MN. The longitudinal force on the bottom of the upper beam increases from 0 to 60 MN, and the longitudinal reaction force on the base also increases from 0 to 60 MN. At 0.02 s, the load applied on the compression-shear test machine frame is suddenly unloaded, and all the acting forces instantly reduces to 0. During 0.01 s~0.02 s, the load remains unchanged. During 0.02 s~0.07 s, it is a dynamic response process after sudden unloading, and the dynamic characteristics of the compression-shear test machine frame after sudden unloading under ultimate working conditions are analyzed during this period.

In the process of stress changing with time, Figures 11–13 show the stress cloud diagram and curve of the upper beam, column, and base after sudden unloading during 0.02 s~0.07 s, respectively. Figure (a) and Figure (b) are the maximum stress cloud diagram of dynamic stress on Figure (c). Figure (c) is the stress curve of maximum dynamic stress on Figure (a) and Figure (b).

As shown in Figures 11(a) and 11(b), the maximum dynamic stress of the original and optimized upper beam is at the contact between the hydraulic cylinder and the upper beam. As shown in Figure 11(c), due to the constraint of dead weight and column, the stress of the upper beam before and after sudden unloading will change greatly, and the dynamic stress after sudden unloading is always less than the

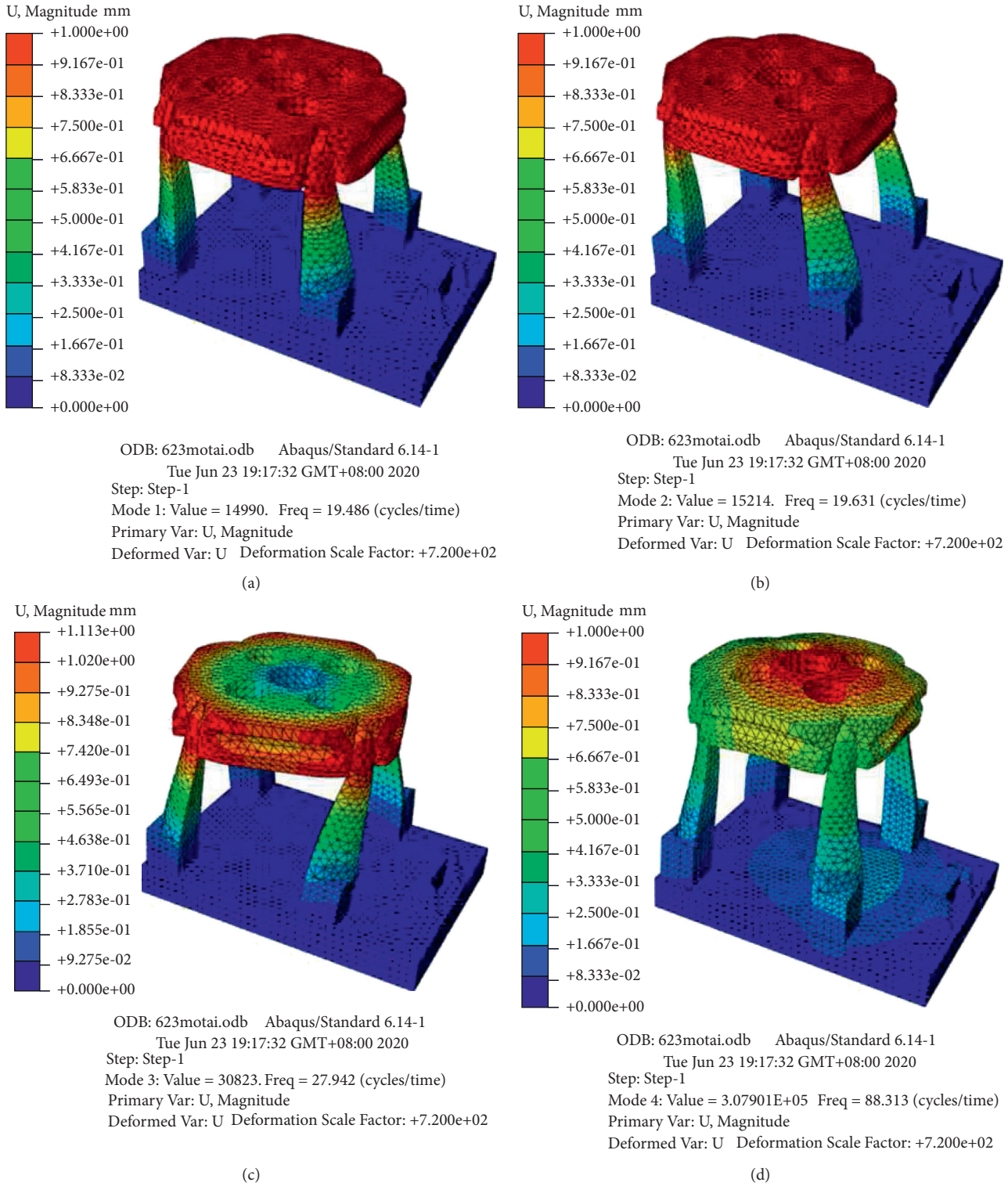

Figure 9: Modal analysis results of compression-shear test machine frame after optimization. (a) First-order mode. (b) Second-order mode. (c) Third-order mode. (d) Fourth-order mode.

static stress before unloading. At 0.039 s, the maximum dynamic stress of the upper beam before optimization is 108.1 MPa. After optimization, the maximum dynamic stress of the upper beam is 140 MPa at 0.047 s. Although the maximum dynamic stress of the optimized upper beam is slightly larger than that before optimization, it is far less than the yield strength of Q345 steel.

As shown in Figures 12(a) and 12(b), the maximum dynamic stress of the column before and after optimization is at the contact position between the column and the upper

Table 2: Comparison of natural frequency of compression-shear test machine frame before and after optimization.

Order number (n)	Natural frequency before optimization (Hz)	Natural frequency after optimization (Hz)
1	24.384	19.486
2	24.626	19.631
3	34.189	27.942
4	90.815	88.313

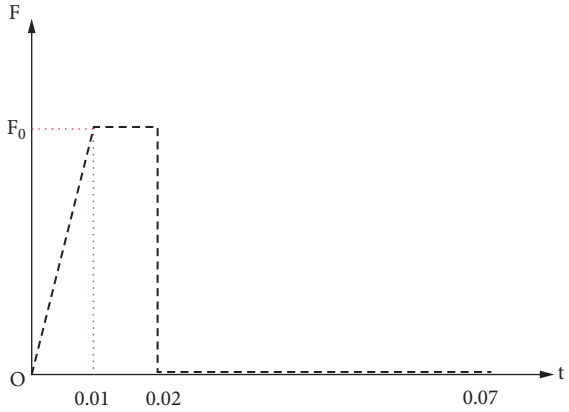

Figure 10: Loading process diagram.

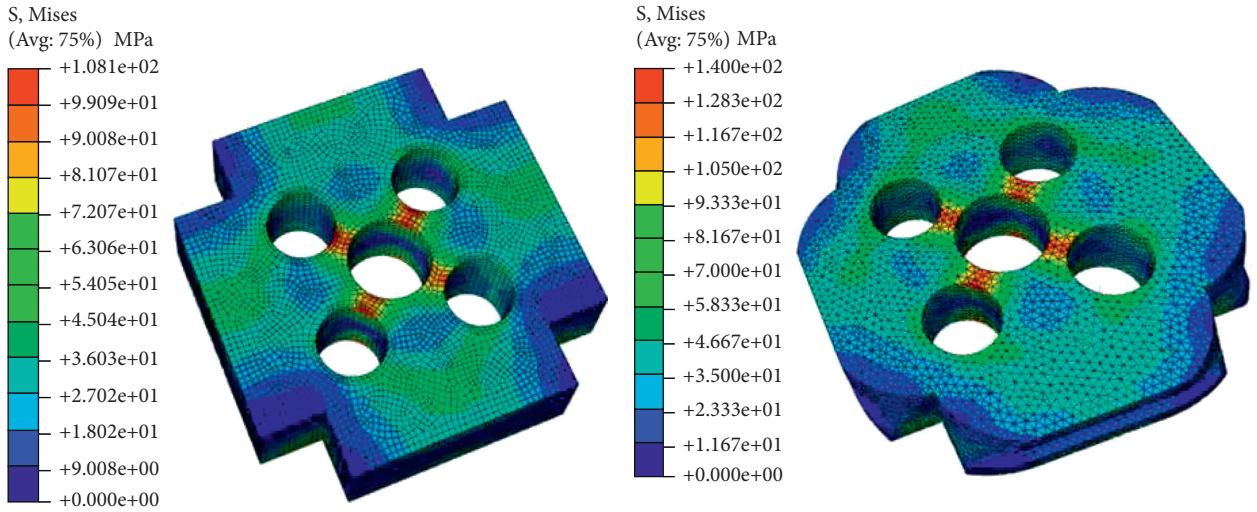

(a) (b)

Figure 11: Continued.

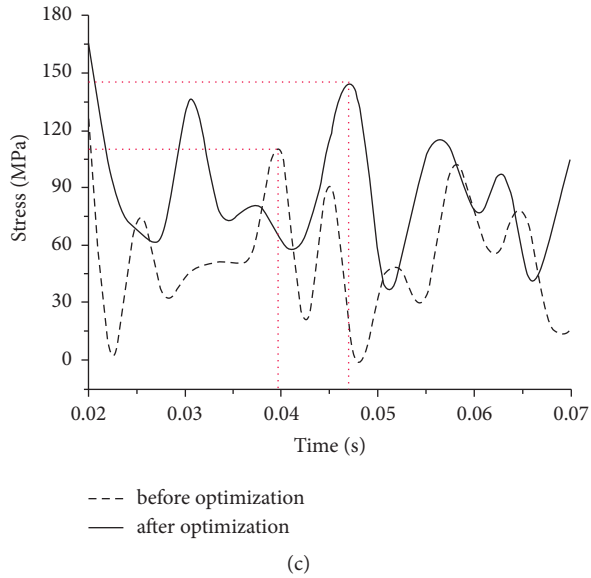

(c)

Figure 11: After sudden unloading, the stress cloud diagram and curve of the upper beam before and after optimization. (a) Stress cloud diagram of upper beam before optimization. (b) Stress cloud diagram of upper beam after optimization. (c) Stress curve of upper beam before and after optimization.

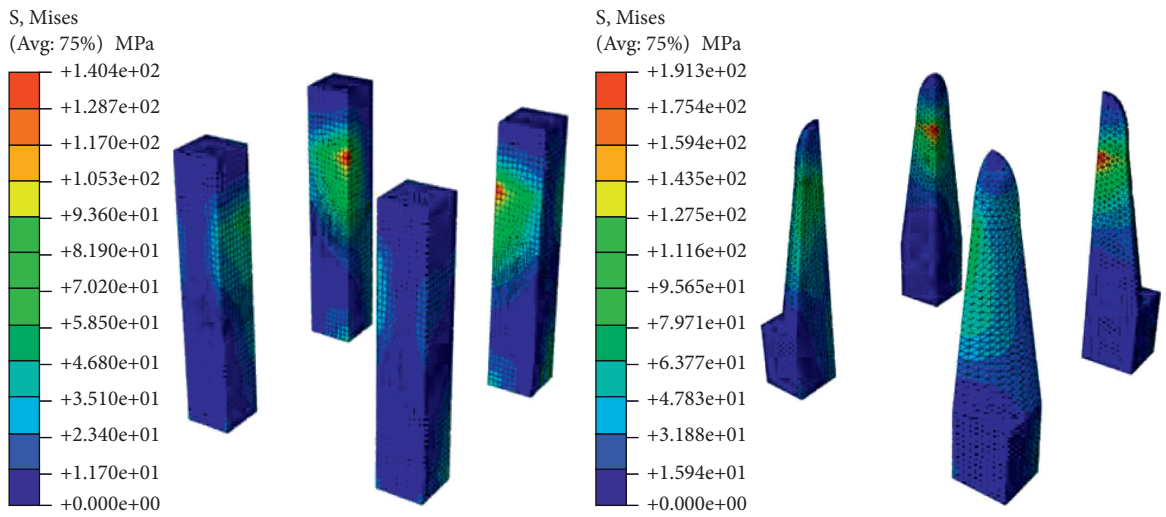

(a) (b)

Figure 12: Continued.

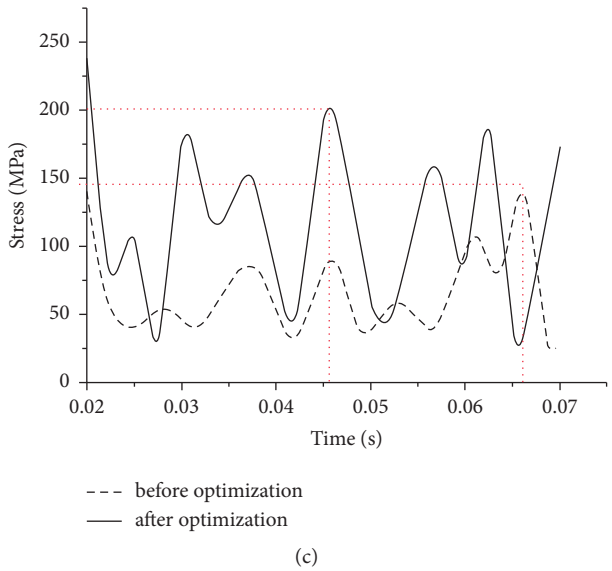

(c)

Figure 12: After sudden unloading, the stress cloud diagram and curve of the front and rear columns before and after optimization. (a) Stress cloud diagram of column before optimization. (b) Stress cloud diagram of column after optimization. (c) Stress curve of column before and after optimization.

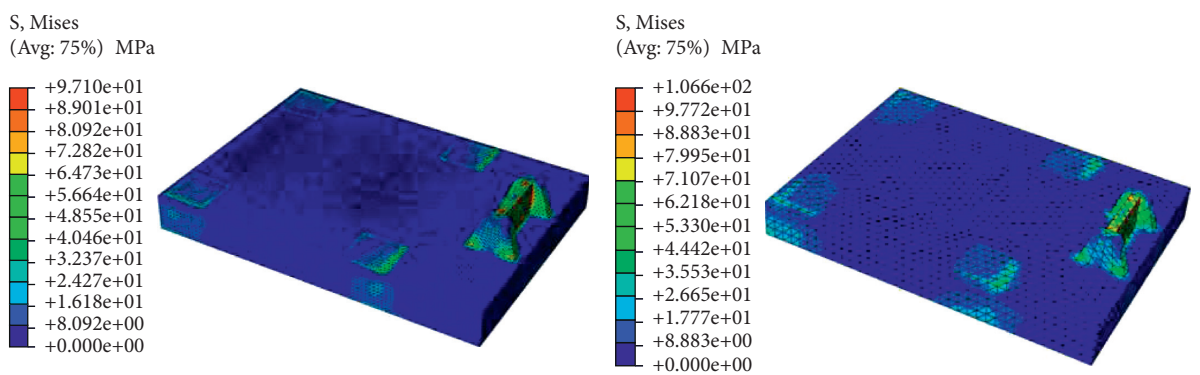

(a) (b)

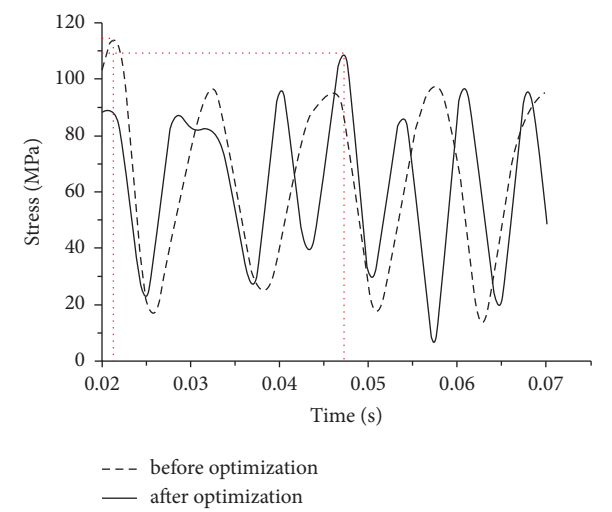

(c)

Figure 13: Stress cloud diagram and curve of the front and rear base of the frame after sudden unloading before and after optimization. (a) Stress cloud diagram of the base before optimization. (b) Stress cloud diagram of the base after optimization. (c) Stress curve of the base before and after optimization.

beam. As shown in Figure 12(c), due to the impact of the beam, the stress of the column after the sudden unloading before and after the optimization will also change greatly. Especially, the dynamic stress of the column before optimization is even greater than the static stress before unloading, whereas after sudden unloading, the dynamic stress of column after optimization is always less than the static stress before unloading. At 0.066 s, the maximum dynamic stress of the column before optimization is 140.4 MPa. After optimization, the maximum dynamic stress of the column base is 191.3 MPa at 0.046 s. Although the maximum dynamic stress of the lightweight column after optimization is greater than that before optimization, it is still far less than the yield strength of Q345 steel.

As shown in Figures 13(a) and 13(b), the maximum dynamic stress of the base is at the cylinder seats before and after optimization. The stress of the base also changes greatly after sudden unloading before and after optimization, and the changing range of the base stress is smaller than that of the upper beam and column as shown in Figure 13(c).

The dynamic stress of the base after sudden unloading before and after optimization is greater than the static stress before unloading. At 0.022 s, the maximum dynamic stress of the base before optimization is 97.1 MPa. After optimization, the maximum dynamic stress of the base is 106.6 MPa at 0.0475 s, which is only slightly larger than that before optimization and far less than the yield strength of Q345 steel.

5. Conclusion

(1) After topology optimization and model reconstructed, the weight of the compression-shear test machine frame reduces by 14.5% compared with that before optimization. The lightweight of the frame is achieved.

(2) After optimization, the maximum static stress of the compression-shear machine frame is still less than the material yield strength, and the maximum displacement is still less than the allowable maximum displacement. The maximum static stress and the maximum displacement meet the requirements of static strength and static stiffness.

(3) After optimization, each mode natural frequency of the compression-shear test machine frame is large, which is far greater than the working frequency. Therefore, the frame will not produce resonance and meet the requirements of dynamic stiffness.

(4) After the machine frame suddenly unloaded, the maximum dynamic stress of the upper beam, column, and base are less than the yield strength of the material after the optimization, which meet the requirement of dynamic strength.

Data Availability

The data used to support the findings of this study are available from the corresponding author upon request.

Conflicts of Interest

The authors declare no conflicts of interest.

Authors' Contributions

Z.H. conceptualized the study; Z.H. and Y.L. investigated the data; G.W., B.C., and C.L. prepared the original draft; G.W., B.C., and S.Z. reviewed and edited the manuscript; J.S., J.Y., and L.C. supervised the study; Z.H., Y.L., and J.S. were involved in funding acquisition.

Acknowledgments

This research was funded by Key Scientific and Technological Project of Henan Transportation Department (2019J2) and Key Scientific and Technological Project of Henan Province (202102110113).

References

[1] X. Y. Sun, W. G. Yang, M. Wang, Y. Wang, Q. Y. Xie, and P. An, "Compression stiffness ratio of rubber bearings under shear deformation," *Engineering Mechanics*, vol. 34, no. 1, pp. 58–68, 2017.

[2] E. Tubaldi, S. A. Mitoulis, and H. Ahmadi, "Comparison of different models for high damping rubber bearings in seismically isolated bridges," *Soil Dynamics and Earthquake Engineering*, vol. 104, pp. 329–345, 2018.

[3] J. Zhao, H. Yoon, and B. D. Youn, "An efficient concurrent topology optimization approach for frequency response problems," *Computer Methods in Applied Mechanics and Engineering*, vol. 347, pp. 700–734, 2019.

[4] H. M. Magid, B. Kamoon, and Z. H. Obaid, "Design sensitivity analysis for identification the optimum shape and geometry optimization by using finite element method," *Journal Mechanics Continua Mathemedical Science*, vol. 11, pp. 315–325, 2019.

[5] J. H. Rong, G. J. Tang, Y. Y. Luo, and D. S. Yang, "A research on the numerical topology optimization technology of large three-dimensional continuum structures considering displacement requirements," *Engineering Mechanics*, vol. 3, pp. 20–27+19, 2007.

[6] X. D. Wang, L. Wang, and Y. Sun, "Electro-hydraulic servo test machine of analysis and optimization based on FEM," *Journal of Changchun University of Technology (Natural Science Edition)*, vol. 39, no. 3, pp. 243–247, 2018.

[7] H. Xue, K. X. Wang, and W. X. Liu, "Optimization design of the connecting rod of the hydraulic fatigue tesing machinne," *J Lanzhou Jiaotong Univ*, vol. 31, no. 4, pp. 71–73, 2012.

[8] G. D. Feng and Y. B. Luo, "Optimization design of main structure of concrete temperature-stress test machine," *Mach Tool Hydraul*, vol. 46, no. 4, pp. 1–5, 2018.

[9] J. Du and N. Olhoff, "Topological design of freely vibrating continuum structures for maximum values of simple and multiple eigenfrequencies and frequency gaps," *Structural and Multidisciplinary Optimization*, vol. 34, no. 2, pp. 91–110, 2007.

[10] G. Kazakis, I. Kanellopoulos, S. Sotiropoulos, and N. D. Lagaros, "Topology optimization aided structural design: interpretation, computational aspects and 3D printing," *Heliyon*, vol. 3, Article ID e00431, 2017.

[11] F. Di Trapani, M. Malavisi, G. C. Marano, A. P. Sberna, and R. Greco, "Optimal seismic retrofitting of reinforced concrete buildings by steel-jacketing using a genetic algorithm-based framework," *Engineering Structures*, vol. 219, Article ID 110864, 2020.

[12] S. Sotiropoulos, G. Kazakis, and N. D. Lagaros, "Conceptual design of structural systems based on topology optimization and prefabricated components," *Computers & Structures*, vol. 226, Article ID 106136, 2020.

[13] F. Di Trapani, A. P. Sberna, and G. C. Marano, "A new genetic algorithm-based framework for optimized design of steel-jacketing retrofitting in shear-critical and ductility-critical RC frame structures," *Engineering Structures*, vol. 243, Article ID 112684, 2021.

[14] M. M. Rosso, R. Cucuzza, F. Di Trapani, and G. C. Marano, "Nonpenalty machine learning constraint handling using PSO-svm for structural optimization," *Advances in Civil Engineering*, vol. 17, 2021.

[15] R. Cucuzza, M. M. Rosso, G. C. Marano, and G. C. Marano, "Optimal preliminary design of variable section beams criterion," *SN Applied Sciences*, vol. 3, no. 8, p. 745, 2021.

[16] L. J. Wang, M. Q. Zhu, X. L. Hu, and M. J. Tang, "Opening design for double-layer concrete box girder based on topology optimization," *Engineering Mechanics*, vol. 37, pp. 282–286, 2019.

[17] Y. S. Kong, S. Abdullah, M. Z. Omar, and S. M. Haris, "Topological and topographical optimization of automotive spring lower seat," *Latin American Journal of Solids and Structures*, vol. 13, no. 7, pp. 1388–1405, 2016.

[18] J. X. Li, J. L. Tan, and J. B. Dong, "Lightweight Design of front suspension upright of electric formula car based on topology optimization method," *World Electr Vehicle J*, vol. 11, 2020.

[19] Y. C. Deng and C. Sun, "Optimization design on plate-rib structure for certain kinds of aircraft," *Materials Research Express*, vol. 6, pp. 209–219, 2008.

[20] C. Zhang, D. J. Jia, F. C. Li, and L. Y. Qin, "Topology optimization design and mechanical property analysis of the transverse bulkhead of a trimaran," *Journal of Harbin Engineering University*, vol. 41, no. 6, pp. 805–811, 2020.

[21] V. R. Resmy and C. Rajasekaran, "Evolutionary topology optimization of structural concrete under various load cases," *Advances in Civil Engineering*, vol. 83, pp. 369–380, 2019.

[22] Y. Wang, W. Liu, and J. Zhang, "Topology optimization design of typical hinge for civil aircraft," *Lecture Notes in Electrical Engineering*, vol. 459, pp. 2872–2881, 2019.

[23] G. Xie, Y. Dong, J. Zhou, and Z. Sheng, "Topology optimization design of hydraulic valve blocks for additive manufacturing," *Proceedings of the Institution of Mechanical Engineers - Part C: Journal of Mechanical Engineering Science*, vol. 234, no. 10, pp. 1899–1912, 2020.

[24] W. H. Chu, X. X. Li, and Y. Y. Ge, "Finite element analysis on the load frame of computer controlled electric universal test machine," *Eng Test*, vol. 050, no. B12, pp. 30–32, 2010.

[25] K. Zou, L. Hou, X. J. Bu, and Y. K. Fang, "Multi-working condition topology optimization of forklift door frames based on working condition risk assessments," *China Mechanical Engineering*, vol. 30, no. 5, pp. 568–577, 2019.

[26] K. H. Chang, *Design Theory and Methods Using CAD/CAE: The Computer Aided Engineering Design Series*, pp. 1–494, Academic Press, Elsevier Science, Cambridge, MA, USA, 2014.

[27] V. Young, O. Mquerin, G. P. Steven, and Y. M. Xie, "3D Bi-diectional evo-lutionary tructural optisation (BESO)," in *Proceedings of the Ausralan Conerence on structual Dtimzion*, pp. 275–282, Sydney, Australia, October 1998.